Remote Sensing of Environment 204 (2018) 524–533

Contents lists available at ScienceDirect

Remote Sensing of Environment

journal homepage: www.elsevier.com/locate/rse

Expansion of major urban areas in the US Great Plains from 2000 to 2009 using satellite scatterometer data

Lan H. Nguyen[a], Son V. Nghiem[c], Geoffrey M. Henebry[a,b,*]

[a] Geospatial Sciences Center of Excellence, South Dakota State University, Brookings, SD 57007, USA
[b] Department of Natural Resource Management, South Dakota State University, Brookings, SD 57007, USA
[c] Jet Propulsion Laboratory, California Institute of Technology, Pasadena, CA 91109, USA

ARTICLE INFO

Keywords:
Urbanization
QuikSCAT
Dense Sampling Method
Impervious surface
LandScan

ABSTRACT

A consistent dataset delineating and characterizing changes in urban environments will be valuable for socio-economic and environmental research and for sustainable urban development. Remotely sensed data have been long used to map urban extent and infrastructure at various spatial and spectral resolutions. Although many datasets and approaches have been tried, there is not yet a universal way to map urban extents across the world. Here we combined a microwave scatterometer (QuikSCAT) dataset at ~1 km posting with percent impervious surface area (%ISA) data from the National Land Cover Dataset (NLCD) that was generated from Landsat data, and ambient population data from the LandScan product to characterize and quantify growth in nine major urban areas in the US Great Plains from 2000 to 2009. Nonparametric Mann-Kendall trend tests on backscatter time series from urban areas show significant expanding trends in eight of nine urban areas with *p*-values ranging 0.032 to 0.001. The sole exception is Houston, which has a substantial non-urban backscatter at the northeastern edge of the urban core. Strong power law scaling relationships between ambient population and either urban area or backscatter power (r^2 of 0.96 in either model) with sub-linear exponents (β of 0.911 and 0.866, respectively) indicate urban areas become more compact with more vertical built-up structure than lateral expansion to accommodate the increased population. Increases in backscatter and %ISA datasets between 2001 and 2006 show agreement in both magnitude and direction for all urban areas except Minneapolis-St. Paul (MSP), likely due to the presence of many lakes and ponds throughout the MSP metropolitan area. We conclude discussing complexities in the backscatter data caused by large metal structures and rainfall.

1. Introduction

The world's urban population has grown rapidly from 746 million in 1950 to 3.9 billion in 2014, a more than five-fold increase (United Nations, 2014). As the world continues fast urbanization, about 6.4 billion people are predicted to live in cities by 2050, accounting for 66% of the world's population. The worldwide urbanization has transformed economic, social, political settings (Yusuf et al., 2001; Soh, 2012; Fang et al., 2015) and increasingly exerts impacts on climate and ecosystems at multiple scales (Zhou et al., 2004; Kaufmann et al., 2007; Imhoff et al., 2010; Seto et al., 2012; Bounoua et al., 2015). Understanding of urban change becomes critical to urban planners and decision-makers responsible for sustainable urban development (Seto et al., 2014).

For many years, urban extent and infrastructure have been mapped using multiple sources of remotely sensed data, from moderate to high spatial and spectral resolutions. Airborne images captured in visible and infrared spectrum are primary data sources to map urban land uses and land covers (LULC). Moderate-to-low spatial resolution sensors, such as Landsat (Masek et al., 2000; Zha et al., 2003; Yuan et al., 2005), AVHRR (Hansen et al., 2000), MODIS (Schneider et al., 2009, 2010; Friedl et al., 2010; Huang et al., 2016), ASTER (Chen et al., 2007; Pu et al., 2008), and SPOT (Zhang et al., 2003; Ferri et al., 2014; Sertel and Akay, 2015), offer long spans of imagery for the analysis of urban changes. A major limitation of moderate resolution imagery is that an image pixel may contain multiple types of land cover that may have multiple uses. Traditional classification methods that assume only one LULC type exists in an image pixel may therefore fail to produce accurate results with moderate resolution imagery (Small, 2005). Spectral Mixture Analysis (SMA) represents the reflectance in each pixel by a linear combination of spectral endmembers, provided an alternative to quantify reflectance properties of the urban mosaics (Adams et al., 1986; Smith et al., 1990). Although the SMA has proved useful for describing urban composition in subsequent studies (Lu and Weng,

* Corresponding author at: Geospatial Sciences Center of Excellence, South Dakota State University, Brookings, SD 57007, USA
E-mail address: geoffrey.henebry@sdstate.edu (G.M. Henebry).

http://dx.doi.org/10.1016/j.rse.2017.10.004
Received 23 December 2016; Received in revised form 15 September 2017; Accepted 5 October 2017
Available online 06 November 2017

2004; Pu et al., 2008; Small, 2001; Wu and Murray, 2003), it is usually designed with spectral endmembers specific to a location or research problem. High spatial resolution images from airborne and space-borne platforms are increasingly used for urban mapping to better separate urban features (Herold et al., 2003; Li and Shao, 2014; Lu et al., 2010; Myint et al., 2011). However, these very high spatial resolution (< 2 m) data are typically available only at a high cost over a small area at infrequent intervals.

In modern societies, urban areas are brightly and densely lit at night, in contrast to the sparser lighting in surrounding rural areas. The nighttime lights datasets generated from DMSP-Operational Linescan System (OLS) and, more recently, the Visible Infrared Imaging Radiometer Suite (VIIRS) are used widely to map human settlement and to infer socioeconomic development (Small et al., 2005; Shi et al., 2014; Zhou et al., 2015). Although the night lights datasets have demonstrated a great potential for urban studies, they still have several limitations, such as blooming effects and light saturation in urban cores leading to high commission error, variation in local lighting habit and technologies, seasonality in usage, and, for the OLS data, limited dynamic range (Doll, 2008; Huang et al., 2014; Small et al., 2011; Small and Elvidge, 2013; Zhang and Seto, 2013). Urban structure can be characterized using LiDAR systems (Yan et al., 2015) or high-resolution images processed with photogrammetric methods (Takaku et al., 2014). Although LiDAR or high-resolution image datasets can have very fine spatial resolution (≤ 1 m), they are only available at a high cost for a few locations and with long return intervals, if any.

While spectral data and night lights imagery only show urban changes in the 2-D plane, both 2-D and 3-D urban infrastructure could be characterized using data collected by synthetic aperture radars (SAR) with encouraging results (Henderson and Xia, 1998; Nghiem et al., 2001; Gamba et al., 2002; Soergel et al., 2003; Dell'Acqua and Gamba, 2006; Boehm and Schenkel, 2006; Dell'Acqua, 2009; Taubenbock et al., 2012; Esch et al., 2013; Zhou et al., 2017). SAR data can have high resolution ranging from 10 to 100 m; however, SAR data are noisy with a large sigma-naught equivalent noise floor and fixed azimuth angle from a side-looking antenna, which cause many confounding complications in urban areas (same building can have a very large difference in backscatter at different azimuth angles). More importantly, a key limitation is that many SAR datasets have been collected piecewise at different times over different areas of the world. The Shuttle Radar Topography Mission (SRTM) provided an extensive SAR data collected between 60°S and 60°N in February 2000, which has a potential use for global infrastructure mapping for year 2000 (Nghiem et al., 2001). TanDEM-X SAR also has an extensive coverage in recent years; however, TanDEM-X data are not freely accessible. There has been no consistent collection of global SAR data consistently at frequent repeated time intervals until the advent of Sentinel-1A and 1B SAR, which were launched in 2014 and 2016, respectively.

In June 1999, NASA launched a satellite scatterometer—QuikSCAT—to fill the gap created by the loss of NSCAT in 1997. With a comparably high spatial resolution that is sufficient to address urban scales, studies have demonstrated the capability of scatterometer data to characterize urban growth and development in both horizontal and vertical directions (Nghiem et al., 2009). The DSM concept and formulation rigorously founded on the Rosette Transform (Nghiem et al., 2009) and its utility has been demonstrated and published in the literature where important and useful conclusions were reported. These include: observation of physical and demographic characteristics of the urban environment (Nghiem et al., 2014), environmental impacts of Beijing urbanization (Jacobson et al., 2015), assessment and projection of groundwater vulnerability to nitrate pollution (Stevenazzi et al., 2015; Stevenazzi et al., 2017), urban change and impacts in Italy (Masetti et al., 2015), and global mega urbanization and formation of urban mega agglomeration (Nghiem, 2015).

Our objective is to characterize changes in urban environments using high spatial resolution QuikSCAT dataset generated by the Dense Sampling Method (DSM) (Nghiem et al., 2009). We extend the use of DSM data to test and demonstrate its capability in monitoring annual growth of nine major urban areas in the US Great Plains from 2000 to 2009. To examine the validity of the DSM data for urban monitoring, we coupled it with two other well-known and widely used satellite products, ambient population distribution from LandScan (Bhaduri et al., 2002; Dobson et al., 2000) and the percent impervious surface area (%ISA) from NLCD (Fry et al., 2011; Homer et al., 2007; Xian et al., 2011), which represent patterns of urbanization from independent sources. Based on %ISA and LandScan population datasets both indicating urban development, we hypothesized that there would be strong correlations between DSM backscatter and impervious surface area and population data. Intense rainfall can also modify the backscatter observed by a scatterometer (Hilburn et al., 2006; Tournadre and Quilfen, 2003) due to increased soil moisture on land (Nghiem et al., 2012; Seto and Iguchi, 2007). To have better understanding of those phenomena, we also examine relationship between QuikSCAT backscatter and rainfall data from the National Oceanic and Atmospheric Administration (NOAA).

2. Study area and data

2.1. Study area

Our study region is the US Great Plains, a vast expanse of flatland dominated by prairie, steppe and grasslands, stretching east to west from the Missouri River to the Rocky Mountains and north to south from the coniferous forests of Canada to the Rio Grande. Here we examined urbanization in the nine largest urban areas of the region by 2010 Census population (Fig. 1), including: Dallas-Fort Worth (TX); Houston (TX); Minneapolis-St Paul (MN); Kansas City (KS-MO); Oklahoma City (OK); Tulsa (OK); Omaha (NE) - Council Bluffs (IA); Wichita (KS); and Des Moines (IA). We chose this study region primarily due to the small variation in topography over the entire Great Plains, which minimizes high average backscatter from terrain effects.

2.2. Data

The SeaWinds scatterometer on QuikSCAT satellite collected daily global data covering 90% of the Earth surface with an original footprint of approximately 25 km in azimuth and 37 km in range. Here, we used QuikSCAT data from 2000 to 2009 processed by the Dense Sampling Method (DSM) (Nghiem et al., 2009). The DSM linearly composes a set of multi-azimuths, thin-slice beams to obtain the radar backscatter data posted in a much finer grid with the pixel scale of about 1 km. The DSM also characterizes backscatter fluctuations of the target in each pixel that arise due to azimuth asymmetry, human activities and environmental changes using the index of variability (IV). As a trade-off, the increased spatial resolution results in a reduction in temporal resolution: the near daily temporal resolution of QuikSCAT is reduced to generate an annual higher spatial resolution product. A time series of the annual product is appropriate to identify changes in a growing urban environment. Moreover, the DSM formulation allows the use of data at both vertical (VV) and horizontal (HH) polarizations, and their variability is included in the standard deviation of the product (Nghiem et al., 2009). While backscatter over ocean can have a significant difference between VV and HH data (Nghiem et al., 1997) due to the surface scattering characteristics, VV and HH backscatter data integrated over all azimuth angles are similar over land because of the volume scattering from objects above surface (rocks, trees, buildings, *etc.*), except in flood inundated areas (Brakenridge et al., 2005). Thus, we used both the HH polarization from the inner beam and the VV polarization from the outer beam of QuikSCAT in the data processed by the DSM for this study.

The Multi-resolution Land Characteristics Consortium (MRLC) has generated the National Land Cover Database (NLCD) for the

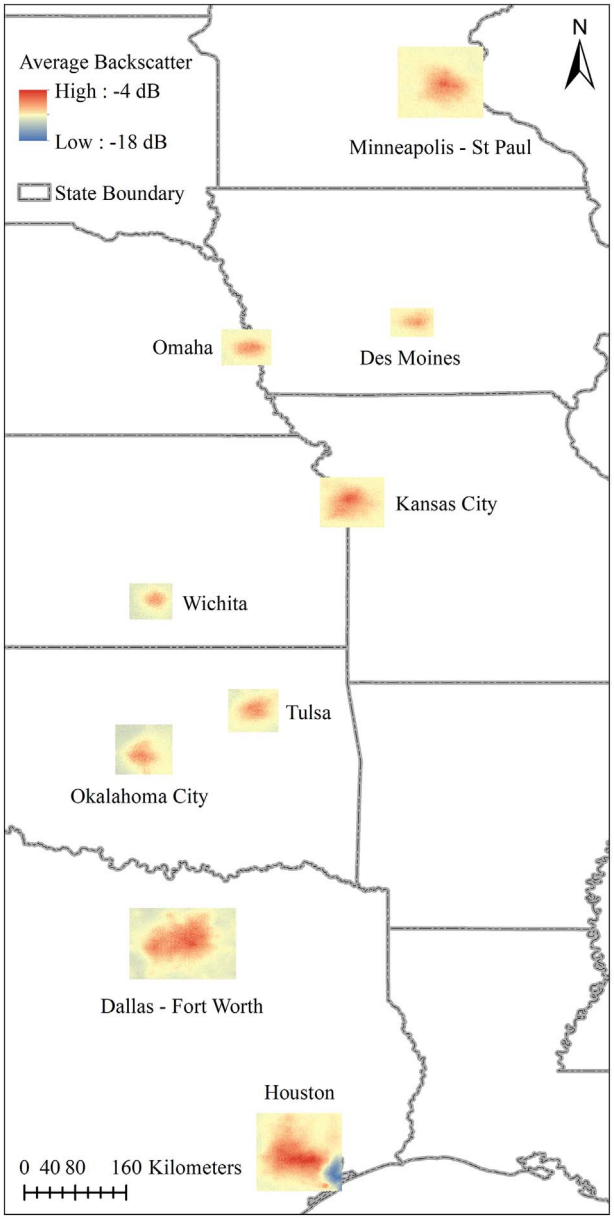

Fig. 1. Nine largest urban areas in the US Great Plains observed by QuikSCAT DSM data.

conterminous United States at 30 m resolution from Landsat data every 5 years since 2001 (Fry et al., 2011; Homer et al., 2007). Two major layers of the NCLD datasets are land cover and percent developed imperviousness (%ISA). In this study, we compared changes in backscatter and impervious surface area (ISA) between 2001 and 2006. The ISA for each pixel was calculated as reported %ISA multiplied by the nominal pixel area of 0.09 ha. The urban area's total impervious surface area is the simple summation of ISA values from all pixels within the defined urban area.

LandScan is a fine spatial resolution (30 arc-second) population distribution database generated by disaggregating census counts at regional and sub-national scale using geospatial data and a multi-variable dasymetric modeling approach (Rose and Bright, 2014). Because data availability and quality vary for each region, the LandScan algorithm was manually corrected to match the regional geographic and demographic conditions. LandScan data represents the "ambient population", that is, the population averaged over 24 h, which combines diurnal activities (*e.g.*, work, travel, shopping, *etc.*) and nocturnal sleeping locations and, thus, more closely corresponds to the active urban population than an approach that counts people only where they sleep (Dobson et al., 2000).

Monthly rainfall data from 2000 to 2009 for 101 stations located within or nearby study areas were downloaded from the NOAA's National Centers for Environmental Information (formerly the National Climatic Data Center). A list of stations and geographic locations is provided in Table S1.

3. Approach

3.1. Characterization of urbanization by DSM data

Urban expansions from 2000 to 2009 in the nine urban areas were characterized by changes in annual backscatter contours. The 5 × 5 Gaussian Kernel Smoothing (with sigma = 1) was applied to reduce noise in the original DSM scatterometer data. We note that the annual DSM data is a continuum in space that can represent continuous rural to urban gradients, while allowing users to define a specific threshold for each specific investigation. We carried out exploratory analyses of the latitudinal and longitudinal distributions of backscatter values with different thresholds across every MSAs, and found that urban pixels would consistently separate from surrounding environment at − 10 dB. Thus, for each of the nine Great Plains cities, the − 10 dB contour serves as a common basis for evaluating progressive urban expansion in the 2000s.

We also coupled backscatter contours with changes in impervious surfaces between 2001 and 2006 to reveal urbanization using two independent sources. For a better visualization, the backscatter contours are displayed in the diverging color ramp from indigo (2000) to dark red (2009) (Figs. 2 & S1–S7). To quantify urbanization over the study period, we first calculated areas covered by each − 10 dB contour. Linear regression and the nonparametric Mann-Kendall (MK) trend test were then applied to the time series to examine the urban expansion associated with each area.

3.2. Comparison between backscatter and population dataset

Many quantitative attributes of cities have been shown to exhibit power law scaling as a function of population size, with superlinear exponent values ($\beta > 1$) for variables related to social characteristics and sublinear exponent values ($\beta < 1$) for variables related to "infrastructure display" (Bettencourt et al., 2007; Bettencourt, 2013). Here, we examined whether DSM backscatter and LandScan ambient population also exhibit power law scaling relationships. First, we merged urban areas captured by 2000–2009 backscatter contours to produce a single largest possible urban boundary for each MSA. We then estimated the − 10 dB area, decadal mean backscatter power (as defined by Eq. (1)) and total ambient population within the − 10 dB extent. The two power law models were fitted using LandScan population (P) as the predictor and area (A) or backscatter power (BKS) as the response variable (Eqs. 2 and 3). Since the magnitude of backscatter signal is proportional to the amount of total built volume (*i.e.*, larger backscatter for higher density of larger buildings and other man-made structures made by heavier materials like steel) (Nghiem et al., 2009; Stevenazzi et al., 2015; Jacobson et al., 2015), we expect to retrieve $\beta < 1$ in both models.

$$BKS_{mean} = 100 * 10^{\frac{\sigma^0_{mean}}{10}} \quad (1)$$

$$A = a_1 P^{\beta 1} \quad (2)$$

$$BKS = a_2 P^{\beta 2} \quad (3)$$

where $\sigma_{mean}{}^0$ is decadal mean (2000–2009) normalized backscatter signals; a_1, a_2 are normalization constants and β1, β2 are scaling exponents of the power law models. In Eq. (1), without loss of generality, we use the number 100 as a proportional coefficient for arbitrary power

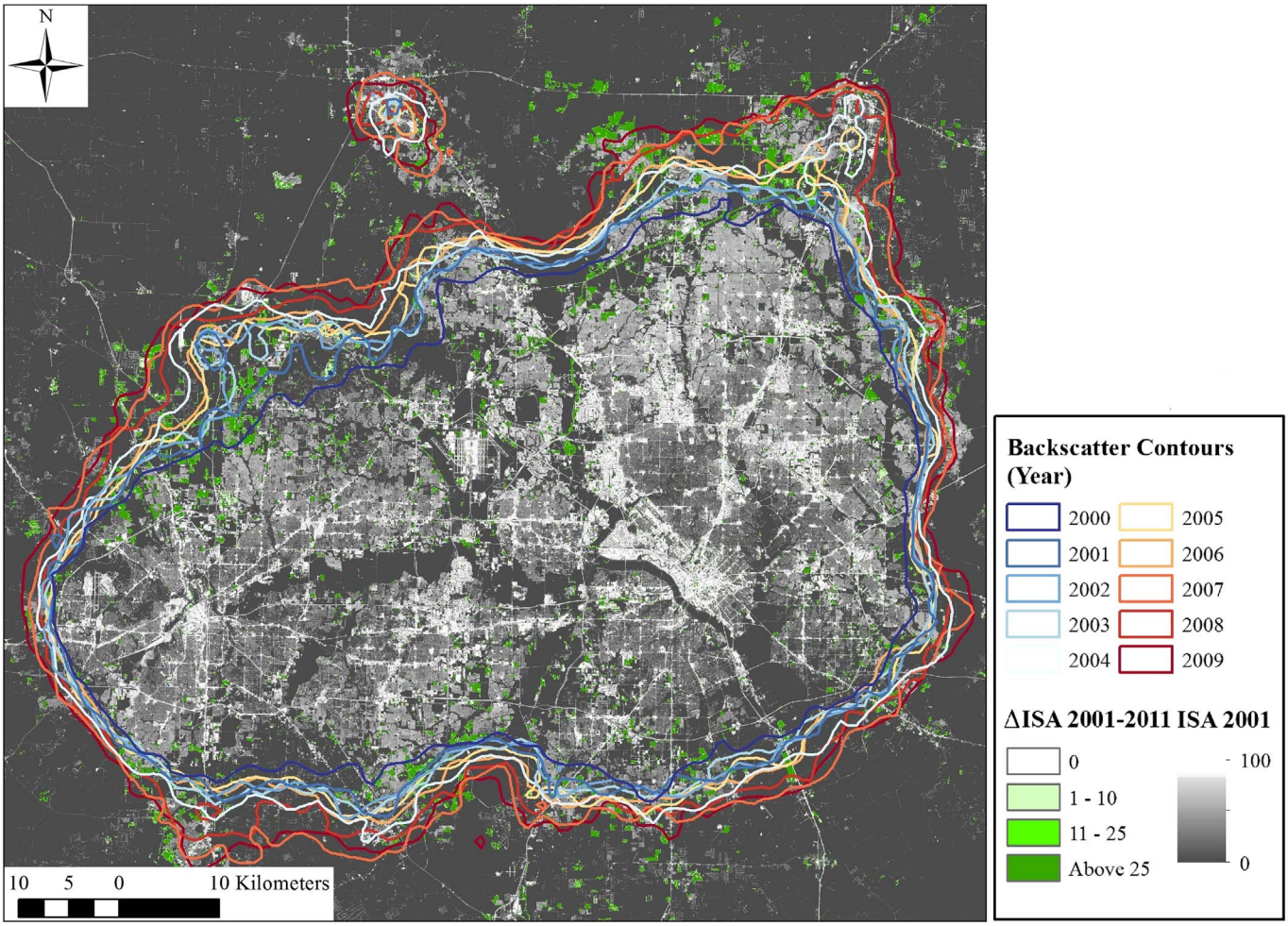

Fig. 2. The − 10 dB backscatter contours in Dallas-Fort Worth, TX. The earlier year contours, from 2000 to 2004, are displayed in cooler colors while the later year contours, from 2005 to 2009, are shown in warmer colors. The 2001%ISA layer, shaded in black-white scale, provides background that aids interpretation of backscatter contours. The open lands with no impervious surfaces (%ISA = 0) and water bodies are shaded in black. Urban (built-up) areas with higher %ISA values are shaded in grey to white colors as the transition from suburban to the urban core. The 2001–2006%ISA changes layer give an idea of where and how quickly urbanization occurs.

units in each pixel.

3.3. Comparison between backscatter and impervious surface area

We focused particularly on horizontal expansion occurring near city boundaries as this expansion front would indicate growth of the built environment. Initially, differences were captured as the area between the − 10 dB backscatter contours in 2001 and 2006. These rings in the nine urban areas represent both urban expansion rate (area of the ring) and major direction of urbanization (maximum distances between two contours). We then generated a buffer of the rings and used those buffers as "evaluation zones" to compare the backscatter and ISA datasets. These evaluation zones were used for comparison instead of the rings for two reasons. First, we used a 5 × 5 smoothing kernel to reduce noise in the original dataset. Therefore, backscatter values at zone edge are affected by values within the 2.5-pixel radius. Second, effects in the DSM backscatter dataset should be considered due to the resultant gain pattern in the DSM data processing. The buffer should neither too small (to compensate for smoothing process) or too large (so that pixels at the edge have weak or no contribution to the backscatter of a central pixel). Originally, we performed the analysis for multiple buffer thresholds from 3 to 5 km at 0.5 km step (in between the size of the smoothing windows and half diameter of the original QuikSCAT footprint). Results were slightly different for each buffer threshold but major conclusions remain the same. Therefore, we reported the analysis for 4.5 km buffer, which showed median values. The same buffer was applied in all cities for a consistent analysis.

To compare between backscatter and impervious area, we first divided the evaluation zones into eight sectors, and then estimated total %ISA and backscatter power increases between 2001 and 2006 within each sector. Next, changes in backscatter power (ΔBKS) were calculated by Eq. (4). The results were plotted and examined by several correlation tests to describe the relationship between ISA and backscatter increases over the nine urban areas.

$$\Delta BKS = BKS_{06} - BKS_{01} = \left(10^{\frac{\sigma^0_{06}}{10}} - 10^{\frac{\sigma^0_{01}}{10}}\right)^* 100 \quad (4)$$

with ${\sigma_{01}}^0, {\sigma_{06}}^0$ being the 2001 and 2006 normalized backscatter signals, respectively.

3.4. Impact of rainfall on backscatter signal

To demonstrate impact of rainfall on backscatter in each study area, we first averaged the monthly rainfall from all available stations (to minimize missing data) and accumulated to the total annual amount. We then used four correlation tests to examine relationship between the total annual rainfall and de-trended area time series, calculated as differences between areas captured by the − 10 dB contours and their fitted linear model values from Section 3.1.

Table 1
Linear models (r^2) and Mann-Kendall trend tests (Tau) for urban areas captured by −10 dB contours. Indication of significance: *, **, and *** for *p*-values < 0.05, 0.01, and 0.001, respectively.

Urban area	r^2	Tau
Dallas-Ft. Worth	0.83***	0.87***
Houston	0.24	0.24
Minneapolis-St. Paul	0.36	0.56*
Kansas City	0.72**	0.64*
Oklahoma City	0.65**	0.60*
Tulsa	0.70**	0.73**
Omaha	0.84***	0.78**
Wichita	0.67**	0.73**
Des Moines	0.83***	0.87***

4. Results

4.1. Urbanization by DSM backscatter data

Fig. 2 demonstrates the capability of the DSM scatterometer dataset to delineate urban extents: the −10 dB contours generally correspond to the limits of built-up areas shown by the 2001%ISA layer. Although contour lines may cross each other, the earlier year contours (displayed in cooler colors) were generally superseded by later year contours (displayed in warmer colors), which represents outward urban expansion through time. This spatial pattern was consistently observed throughout all studied areas (Figs. 2 and S1–S7). Backscatter contours were also able to show urban expansion in both magnitude and direction. In Dallas-Fort Worth, urbanization occurred mostly in the northern half, indicated by the larger distance between 2000 (blue) and 2009 (red) contours. We also observed more ISA changes between 2001 and 2006 in the northern parts of both urban areas.

Temporal trends of urban areas covered by the 2000–2009 contours were assessed using linear regression and the nonparametric Mann-Kendall (MK) trend test (Table 1). The MK tests indicated statistically significant growth of every study city, except Houston. Coefficients of determination (Fig. 3 & Table 1) varied among areas from 0.24 to 0.84 indicating strong variation in 10 years of urban growth in some urban areas. Although the Minneapolis-St Paul model was significant ($p < 0.05$), it exhibited a markedly lower coefficient of determination ($r^2 = 0.36$).

4.2. Comparison between DSM backscatter and LandScan data

The strong positive relationships between ambient population and area or backscatter power are evident (Figs. 4, 5). Although the quantities for area and backscatter power were both derived from the DSM data, they are not quite the same. While urban area only demonstrates

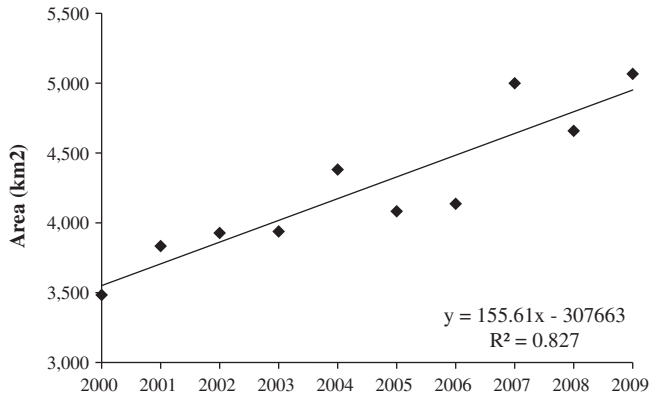

Fig. 3. Urbanization in Dallas-Fort Worth between 2000 and 2009 captured by −10 dB backscatter contours.

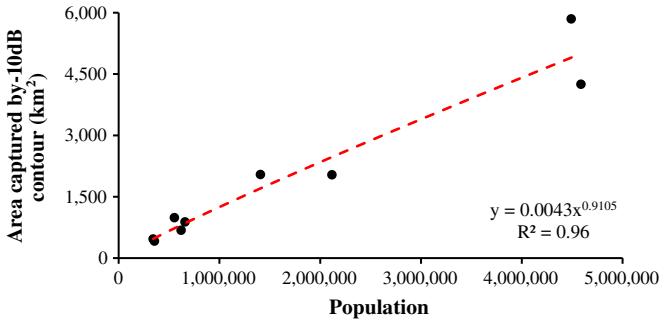

Fig. 4. The relationship between areas captured by decadal mean backscatter and LandScan ambient population for nine largest urban areas in the US Great Plains.

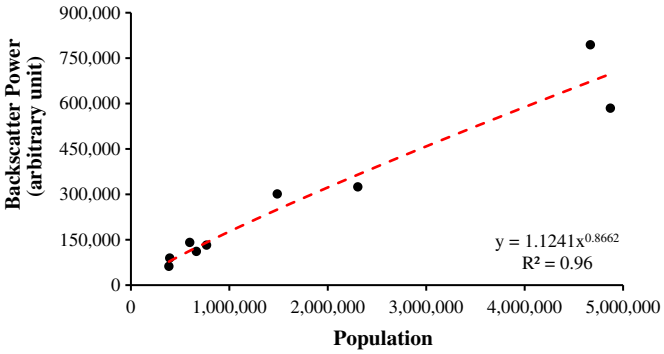

Fig. 5. The relationship between decadal mean backscatter power and LandScan ambient population for the nine largest urban areas in the US Great Plains.

lateral limit of the city, the amount of backscatter power in each city is a function of both urban extent and structural characteristics (*e.g.*, building height, density, and construction materials) (Nghiem et al., 2009; Stevenazzi et al., 2015; Jacobson et al., 2015). Scaling exponents (β) in both models were sub-linear (β < 1), and the backscatter-population relationship (Fig. 5) has slightly lower β value than the area-population relationship (Fig. 4) (0.866 *vs.* 0.911). This pattern suggests that as population increases, urban areas become more compact (more vertical than lateral expansion to accommodate the increased population).

4.3. Sectoral analysis

Fig. 6 displays backscatter and impervious areal increases between 2001 and 2006 in Dallas-Fort Worth. There is a strong correlation evident between the two datasets. In areas with larger ISA increases (in shades of red or dark red), we observed larger increases in backscatter power (in shades of green to dark green). Fig. 6 suggests that urban expansion has occurred mostly in the northern half of Dallas-Fort Worth. Fig. 7 demonstrates a strong positive correlation between directional BKS and ISA increases in Dallas-Fort Worth, except for the NW-N direction. Comparisons of increases in backscatter and impervious surface area for eight other studied areas are presented in Supplemental Information (Figs. S8–S15, S16). Table 2 summarizes correlations between 2001 and 2006 sectoral backscatter power and impervious surface area in the nine studied areas. Major urban areas in the Great Plain (other than Minneapolis-St. Paul) show moderate to strong correlation between impervious surface area and backscatter power with the coefficients of determination (r^2) ranging from 0.62 to 0.88, the Pearson correlation coefficients (cor) ranging from 0.79 to 0.94, the Spearman rank correlation coefficients (rho) ranging from 0.52 to 0.98, and the Kendall rank correlation coefficients (tau) ranging from 0.43 to 0.93 (Table 2).

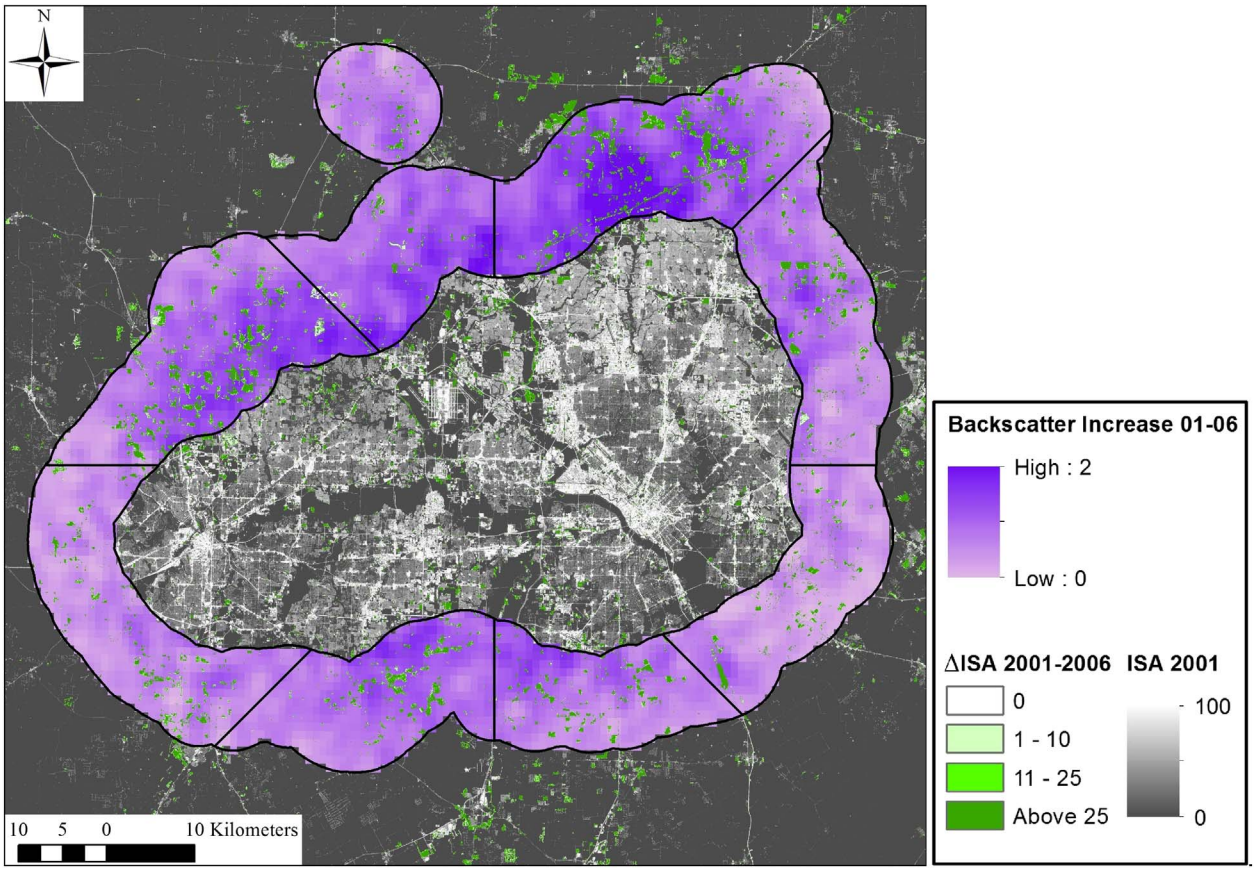

Fig. 6. A comparison of backscatter power (BKS) and increases in percent impervious surface area (%ISA) between 2001 and 2006 in Dallas-Fort Worth.

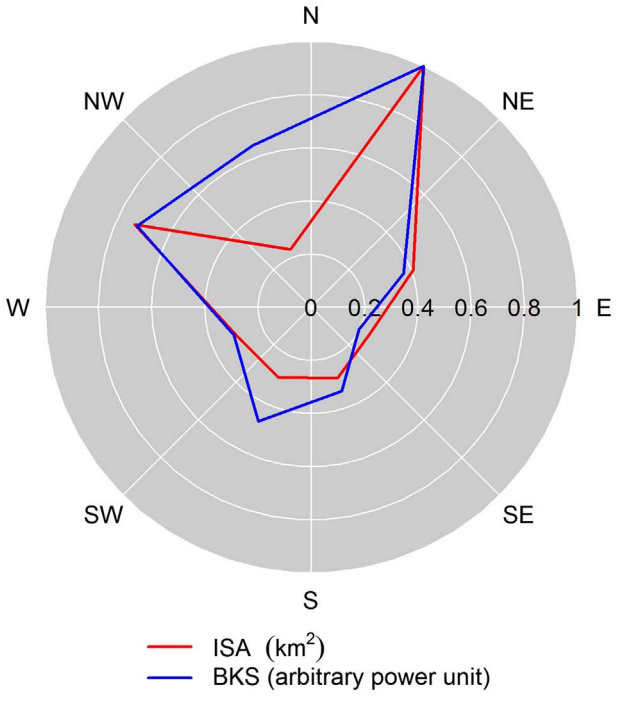

Fig. 7. Sectoral comparison between increased backscatter power (BKS) and increased impervious surface area (ISA) from 2001 to 2006 for Dallas-Fort Worth, TX. ISA and BKS were normalized to aid comparison.

Table 2
Correlations between directional BKS and ISA increases for the 9 urban areas.

Urban area	r^2	cor	rho	tau
Dallas-Ft. Worth	0.70**	0.84**	0.52	0.43
Houston	0.83**	0.91**	0.90**	0.79**
Minneapolis-St. Paul	0.38	0.62	0.40	0.36
Kansas City	0.87***	0.94***	0.98***	0.93***
Oklahoma City	0.87***	0.93***	0.88**	0.71*
Tulsa	0.62*	0.79*	0.67	0.50
Omaha	0.68*	0.82*	0.88**	0.71*
Wichita	0.79**	0.89**	0.76*	0.57
Des Moines	0.88***	0.94***	0.95**	0.86**

r^2: coefficient of determination in linear model, cor: Pearson product-moment correlation coefficient, rho: Spearman rank correlation coefficient, tau: Kendall rank correlation coefficient. Indication of significance: *, **, and *** for *p*-values < 0.05, 0.01, and 0.001, respectively.

4.4. Impacts of rainfall on backscatter signal

A relationship between rainfall and variability in areal fluctuations was evident and consistent throughout the four correlation measurements (Table 3). For example, in Dallas–Fort Worth, the years with higher rainfall (*viz.*, 2004, 2007, 2009) also have larger areas in the − 10 dB contour compared to expectation from a linear model (Fig. 8). On the other hand, the − 10 dB contour areas are smaller in years with lower rainfall amount (*viz.*, 2005, 2006, 2008). Similar situations were observed in other urban areas (Fig. S19). Areas with larger urban extent tend to show higher correlation between detrended areas and total annual rainfall (Table 3).

Table 3
Correlations between detrended area time series and annual rainfall.

Urban Area	r^2	cor	rho	tau
Dallas-Ft. Worth	0.71**	0.84**	0.84**	0.69**
Houston	0.67**	0.82**	0.83**	0.60*
Minneapolis-St. Paul	0.00	0.07	− 0.13	− 0.11
Kansas City	0.51*	0.72*	0.68*	0.47
Oklahoma City	0.58*	0.76*	0.66*	0.47
Tulsa	0.26	0.51	0.54	0.42
Omaha	0.14	0.38	0.49	0.38
Wichita	0.32	0.56	0.55	0.38
Des Moines	0.09	0.30	0.38	0.33

r^2: coefficient of determination in linear model, cor: Pearson product-moment correlation coefficient, rho: Spearman rank correlation coefficient, tau: Kendall rank correlation coefficient. Indication of significance: *, **, and *** for *p*-values < 0.05, 0.01, and 0.001, respectively.

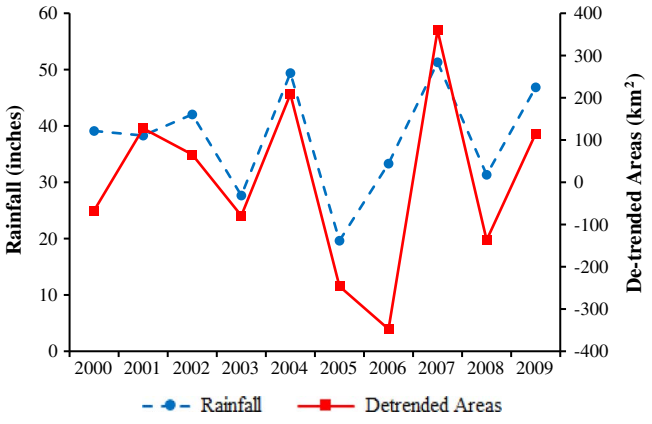

Fig. 8. Total annual rainfall and detrended area time series in Dallas-Fort Worth, TX.

5. Discussion

The contours of backscatter power could illustrate urban growth both in rate and direction. For noise reduction in the DSM backscatter data, we smoothed data before generating contours to enhance visual interpretation. Differences between backscatter of built-up and non-built-up pixels were less significant after smoothing: backscatter from built-up areas reduced while backscatter from non-built-up pixels increased. The tradeoff for better visualization is increased spatial dependence in the dataset, which affected the sectoral analysis. For example, in Figs. 6 and 7, the NW-N portion had low ISA value but large backscatter power. The smoothing process partially included the high backscatter values from the N-NE and W-NW portions. Across the nine urban areas, we can see instances where the − 10 dB contours may run through areas shaded in dark grey that have very little or no impervious surfaces (Figs. 2, 9, S1–S7).

Although the DSM data show the overall capability to study urban and suburban environments, it is necessary to examine limitations of DSM signatures in addition to relatively coarse spatial resolution. Backscatter can be strongly affected by some special structures, especially large structures made of metal. Strong scattering back from a single structure, such as an electrical power transmission tower or a metal-roofed warehouse, can potentially dominate an entire 1 km pixel. Even in high spatial resolution optical imagery, it can be very difficult to distinguish a transmission tower from background objects. In the original backscatter images, we found several areas across the nine urban areas that did not seem to have many structures, but still returned strong backscatter. One large building (*e.g.*, factory, warehouse, distribution center, megastore, *etc.*), rather than the total number of small residential houses, may dominate the backscatter in the given pixel. Considered as a built-up pocket of urbanization, such a case has also been observed in Florence, Italy, where a new dominant building may be permitted for construction in an isolated vacant land lot in the historical city (Masetti et al., 2015). A sample of original average backscatter is provided in Fig. S17.

In addition, the occurrence of numerous open water surfaces within the urban area was found to complicate the backscatter signature. For example, lake water surfaces can exhibit a large range of backscatter depending on wind speed and wind direction (Nghiem et al., 2004). Many open water bodies are distributed across the Minneapolis-St. Paul area (Fig. S18), and complex interactions between weather, water bodies, and the radar responses may result in the high interannual variation in backscatter observed for MSP (Table 1). Furthermore, if water surfaces are located nearby solid subjects such as stands of trees or buildings, a double-bounce interaction can occur, resulting in high backscatter (Rykhus and Lu, 2007). Such effects may have occurred near Liberty, TX (Fig. 9) as the Trinity River crosses the middle of this area. In addition, Trinity River may also spread across the floodplain during the rainy season. During a flood, the water surface may be mixed with trees and buildings, thus potentially enhancing the backscatter through double-bounce interactions.

Our analysis supported previous findings that intense rainfall can alter the backscatter (Hilburn et al., 2006; Tournadre and Quilfen, 2003). Table 3 indicated a stronger effect in larger cities where rainwater caught over a large area is more consistent than that over a small city extent where precipitation data suffer significantly from inconsistencies due to anomalous propagation, point measurement, and local virga (Nghiem et al., 2012). We may be able to take advantage of the detrended areal fluctuations of the DSM results to quantify inter-annual rainfall variation in urban areas where decadal rainfall data may not be available or accessible.

6. Conclusion

A better understanding of urban change is critical to enable sustainable growth and management of urban areas. Here we have demonstrated how microwave scatterometer data processed with the Dense Sampling Method can be used to study urban change in nine major cities in the Great Plains of the United States of America from 2000 and 2009. Active microwave signatures from QuikSCAT enable consistent observations over areas with pervasive or persistent cloud cover and at night in every season. Our results indicate that DSM data can characterize urban expansion both in area and in lateral direction. Between 2000 and 2010, many counties in the US Great Plains were losing population; however, the overall population in the Great Plains increased due to the growth of major urban areas, especially in Dallas-Fort Worth and Houston, where population gains were among the highest in the nation (23.4% and 26.1%, respectively) with 1.2 million more people in urban areas in 2010 than 2000 (Mackun and Wilson, 2011). Using the DSM data, we also observed significant expansion in eight of nine major urban areas, with the sole exception of Houston, likely due to the backscatter anomaly near Liberty, TX. In Dallas-Fort Worth and Houston, the two largest urban areas in the Great Plains, with 2010 population of 6.4 and 6.0 million, respectively (Mackun and Wilson, 2011), urban expansion occurred more in the northern half of each metropolitan area with 68% and 56% increases in backscatter power between 2000 and 2009 for Dallas-Fort Worth and Houston, respectively.

We also encountered complexities in the DSM data. First, interactions between extensive water surface and buildings or other structures can impact backscatter signals over an area (*e.g.*, Houston and Minneapolis-St. Paul). Second, rainfall may increase backscatter to enlarge the area in the − 10 dB reference contour. These complexities indicate that using DSM backscatter alone as a single parameter can incur uncertainties in delineating urban extent.

Past research has shown that DSM data have strong relationships with both nighttime lights and census data (Nghiem et al., 2009). This

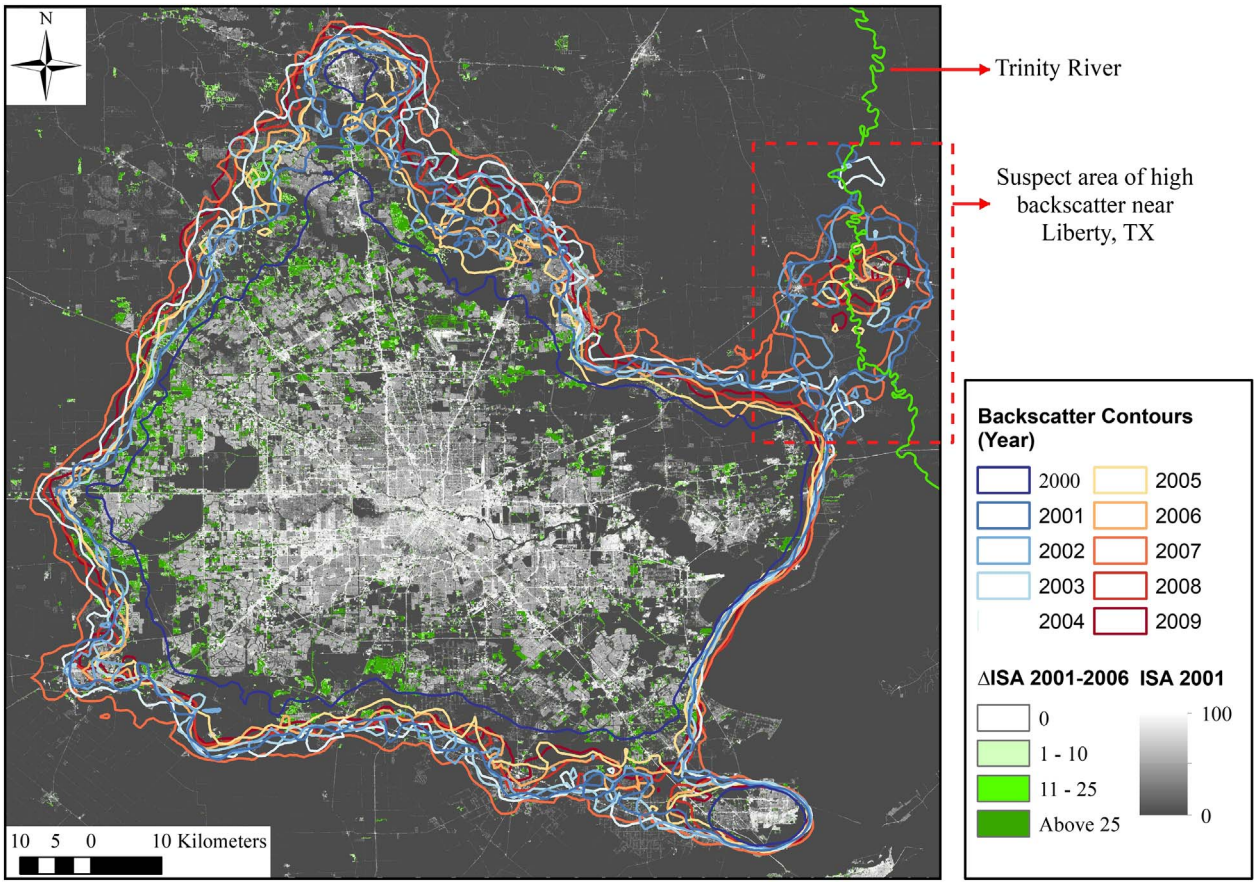

Fig. 9. The −10 dB backscatter contours in Houston, TX. A peculiar area of high backscatter occurs near Liberty, TX. Visual inspection of the area using Google Earth did not reveal large structures that could account for the high backscatter.

study demonstrates strong relationships between the DSM backscatter data and both impervious surface area and ambient population distribution. DSM backscatter data can be, therefore, complementary to other datasets, such as visible to near-infrared spectral data (Small and Nghiem, 2016) or the DSM Index of Variability (IV) metric (Nghiem et al., 2009; Jacobson et al., 2015), to better characterize areas of urban change.

Abbreviations

DSM	Dense Sampling Method
IV	Index of Variability (derived with DSM)
NSCAT	NASA Scatterometer
QuikSCAT	Quick Scatterometer
BKS	Backscatter Power
MRLC	Multi-Resolution Land Characteristics Consortium
NLCD	National Land Cover Database
ISA	Impervious Surface Areas
NOAA	National Oceanic and Atmospheric Administration

Acknowledgments

Funds were available to support in part this research and its publication from NASA grants NNX12AM89G and NNX14AJ32G to GMH. The research carried out at the Jet Propulsion Laboratory, California Institute of Technology, was supported by the NASA Land-Cover and Land-Use Change (LCLUC) Program.

Appendix A. Supplementary data

Supplementary data to this article can be found online at https://doi.org/10.1016/j.rse.2017.10.004.

References

Adams, J.B., Smith, M.O., Johnson, P.E., 1986. Spectral mixture modeling: a new analysis of rock and soil types at the Viking lander 1 site. J. Geophys. Res. 91 (B8), 8098–8112.
Bettencourt, L.M., 2013. The origins of scaling in cities. Science 340 (6139), 1438–1441.
Bettencourt, L.M.A., Lobo, J., Helbing, D., Kühnert, C., West, G.B., 2007. Growth, innovation, scaling, and the pace of life in cities. Proc. Natl. Acad. Sci. 104, 7301–7306.
Bhaduri, B.L., Bright, E.A., Coleman, P.R., Dobson, J.E., 2002. LandScan: locating people is what matters. Geoinformatics 5 (2), 4–37.
Boehm, C., Schenkel, R., 2006, March. Analysis of spatial patterns of urban areas using high resolution polarimetric SAR. In: 1st EARSeL Workshop of the SIG Urban Remote Sensing. Berlin, Germany.
Bounoua, L., Zhang, P., Mostoyoy, G., Thorne, K., Masek, J., Imhoff, M., Shepherd, M., Quattrochi, D., Santanello, J., Silva, J., Wolfe, R., 2015. Impact of urbanization on US surface climate. Environ. Res. Lett. 10 (8), 084010.
Brakenridge, G.R., Nghiem, S.V., Anderson, E., Chien, S., 2005. Space-based measurement of river runoff. EOS Trans. Am. Geophys. Union 86 (19), 185–188.
Chen, Y., Shi, P., Fung, T., Wang, J., Li, X., 2007. Object-oriented classification for urban land cover mapping with ASTER imagery. Int. J. Remote Sens. 28 (20), 4645–4651.
Dell'Acqua, F., 2009. The Role of SAR Sensors. In: Gamba, P., Herold, M. (Eds.), Global Mapping of Human Settlement: Experiences, Datasets, and Prospects. CRC Press, Taylor and Francis, pp. 309–319.
Dell'Acqua, F., Gamba, P., 2006. Discriminating urban environments using multiscale texture and multiple SAR images. Int. J. Remote Sens. 27 (18), 3797–3812.
Dobson, J.E., Bright, E.A., Coleman, P.R., Durfee, R.C., Worley, B.A., 2000. A global population database for estimating populations at risk. Photogramm. Eng. Remote. Sens. 66 (7), 849–857.
Doll, Christopher, 2008. CIESIN Thematic Guide to Night-time Light Remote Sensing and its Applications. Center for International Earth Science Information Network of Columbia University, Palisades, NY.
Esch, T., Marconcini, M., Felbier, A., Roth, A., Heldens, W., Huber, M., Schwinger, M., Taubenbock, H., Muller, A., Dech, S., 2013. Urban footprint processor-fully

automated processing chain generating settlement masks from global data of the TanDEM-X mission. IEEE Geosci. Remote Sens. Lett. 10 (6), 1617–1621.
Fang, C., Liu, H., Li, G., Sun, D., Miao, Z., 2015. Estimating the impact of urbanization on air quality in China using spatial regression models. Sustainability 7 (12), 15570–15592.
Ferri, S., Syrris, V., Florczyk, A., Scavazzon, M., Halkia, M., Pesaresi, M., 2014. A new map of the European settlements by automatic classification of 2.5 m resolution SPOT data. In: 2014 IEEE International Geoscience and Remote Sensing Symposium (IGARSS), pp. 1160–1163.
Friedl, M.A., Sulla-Menashe, D., Tan, B., Schneider, A., Ramankutty, N., Sibley, A., Huang, X., 2010. MODIS collection 5 global land cover: algorithm refinements and characterization of new datasets. Remote Sens. Environ. 114 (1), 168–182.
Fry, J., Xian, G., Jin, S., Dewitz, J., Homer, C., Yang, L., Barnes, C., Herold, N., Wickham, J., 2011. Completion of the 2006 National Land Cover Database for the conterminous United States. Photogramm. Eng. Remote. Sens. 77 (9), 858–864.
Gamba, P., Dell Acqua, F., Houshmand, B., 2002. SRTM data characterization in urban areas. Int. Arch. Photogramm. Remote. Sens. Spat. Inf. Sci. 34 (3/B), 55–58.
Hansen, M.C., DeFries, R.S., Townshend, J.R., Sohlberg, R., 2000. Global land cover classification at 1 km spatial resolution using a classification tree approach. Int. J. Remote Sens. 21 (6–7), 1331–1364.
Henderson, F.M., Xia, Z., 1998. Radar applications in urban analysis, settlement detection and population estimation. Man. Remote. Sens. 2, 759–761.
Herold, M., Scepan, J., Müller, A., Günther, S., 2003. Object-oriented mapping and analysis of urban land use/cover using IKONOS data. In: 22nd EARSeL Symposium Geoinformation for European-Wide Integration, pp. 4–6.
Hilburn, K.A., Wentz, F.J., Smith, D.K., Ashcroft, P.D., 2006. Correcting active scatterometer data for the effects of rain using passive radiometer data. J. Appl. Meteorol. Climatol. 45 (3), 382–398.
Homer, C., Dewitz, J., Fry, J., Coan, M., Hossain, N., Larson, C., Herold, N., McKerrow, A., VanDriel, J.N., Wickham, J., 2007. Completion of the 2001 National Land Cover Database for the conterminous United States. Photogramm. Eng. Remote. Sens. 73 (4), 337–341.
Huang, Q., Yang, X., Gao, B., Yang, Y., Zhao, Y., 2014. Application of DMSP/OLS nighttime light images: a meta-analysis and a systematic literature review. Remote Sens. 6 (8), 6844–6866.
Huang, X., Schneider, A., Friedl, M.A., 2016. Mapping sub-pixel urban expansion in China using MODIS and DMSP/OLS nighttime lights. Remote Sens. Environ. 175, 92–108.
Imhoff, M.L., Zhang, P., Wolfe, R.E., Bounoua, L., 2010. Remote sensing of the urban heat island effect across biomes in the continental USA. Remote Sens. Environ. 114 (3), 504–513.
Jacobson, M., Nghiem, S.V., Sorichetta, A., Whitney, N., 2015. Ring of impact from the mega-urbanization of Beijing between 2000 and 2009. J. Geophys. Res. Atmos. 120 (12), 5740–5756.
Kaufmann, R.K., Seto, K.C., Schneider, A., Liu, Z., Zhou, L., Wang, W., 2007. Climate response to rapid urban growth: evidence of a human-induced precipitation deficit. J. Clim. 20 (10), 2299–2306.
Li, X., Shao, G., 2014. Object-based land-cover mapping with high resolution aerial photography at a county scale in Midwestern USA. Remote Sens. 6 (11).
Lu, D., Weng, Q., 2004. Spectral mixture analysis of the urban landscape in Indianapolis with Landsat ETM imagery. Photogramm. Eng. Remote. Sens. 70 (9), 1053–1062.
Lu, D., Hetrick, S., Moran, E., 2010. Land cover classification in a complex urban-rural landscape with QuickBird imagery. Photogramm. Eng. Remote. Sens. 76 (10), 1159–1168.
Mackun, P., Wilson, S., 2011. Population Distribution and Change: 2000 to 2010 (2010 Census Briefs). United States Census Bureau Available online: https://www.census.gov/prod/cen2010/briefs/c2010br-01.pdf.
Masek, J.G., Lindsay, F.E., Goward, S.N., 2000. Dynamics of urban growth in the Washington DC metropolitan area, 1973–1996, from Landsat observations. Int. J. Remote Sens. 21 (18), 3473–3486.
Masetti, M., Nghiem, S.V., Sorichetta, A., Stevennazi, S., Fabbri, P., Pola, M., Filippini, M., Brakenridge, G.R., 2015. Urbanization affects air and water in Italy's Po plain. EOS, Earth. Space Sci. News 96 (21), 13–16.
Myint, S.W., Gober, P., Brazel, A., Grossman-Clarke, S., Weng, Q., 2011. Per-pixel vs. object-based classification of urban land cover extraction using high spatial resolution imagery. Remote Sens. Environ. 115 (5), 1145–1161.
Nghiem, S.V., 2015. Global mega urbanization and impacts in the 2000s. In: Proceedings IEEE International Geoscience and Remote Sensing Symposium. Milan, Italy, pp. 83–85.
Nghiem, S.V., Li, F.K., Neumann, G., 1997. The dependence of ocean backscatter at Ku-band on oceanic and atmospheric parameters. IEEE Trans. Geosci. Remote Sens. 35 (3), 581–600.
Nghiem, S.V., Balk, D., Small, C., Deichmann, U., Wannebo, A., Blom, R., Sutton, P., Yetman, G., Chen, R., Rodriguez, E., Houshmand, B., Neumann, G., 2001. Global infrastructure: The potential of SRTM data to break new ground. In: Jet Propulsion Laboratory Document D-23049, pp. 23 (Pasadena, CA).
Nghiem, S.V., Leshkevich, G.A., Stiles, B.W., 2004. Wind fields over the Great Lakes measured by the SeaWinds scatterometer on the QuikSCAT satellite. J. Great Lakes Res. 30 (1), 148–165.
Nghiem, S.V., Balk, D., Rodriguez, E., Neumann, G., Sorichetta, A., Small, C., Elvidge, C., 2009. Observations of urban and suburban environments with global satellite scatterometer data. ISPRS J. Photogramm. Remote Sens. 64 (4), 367–380.
Nghiem, S.V., Wardlow, B.D., Allured, D., Svoboda, M.D., LeComte, D., Rosencrans, M., Chan, K.S., Neumann, G., 2012. Microwave remote sensing of soil moisture – science and applications. In: Wardlow, B.D., Anderson, M.C., Verdin, J.P. (Eds.), Remote Sensing of Drought – Innovative Monitoring Approaches. CRC Press, Taylor and Francis, pp. 197–226.
Nghiem, S.V., Sorichetta, A., Elvidge, C.D., Small, C., Balk, D., Deichmann, U., Neumann, G., 2014. Urban environments, Beijing case study. In: Njoku, E. (Ed.), Encyclopedia of Remote Sensing. Springer, Heidelberg, Germany, pp. 869–878.
Pu, R., Gong, P., Michishita, R., Sasagawa, T., 2008. Spectral mixture analysis for mapping abundance of urban surface components from the Terra/ASTER data. Remote Sens. Environ. 112 (3), 939–954.
Rose, A.N., Bright, E.A., 2014. The Landscan Global Population Distribution Project: current state of the art and prospective innovation. In: Paper Presented at the Population Association of America Annual Meeting, Boston, MA, Available online: http://paa2014.princeton.edu/papers/143242.
Rykhus, R., Lu, Z., 2007. Hurricane Katrina flooding and oil slicks: mapped with satellite imagery. In: Farris, G.S., Smith, G.J., Crane, M.P., Demas, C.R., Robbins, L.L., Lavoie, D.L. (Eds.), Science and the Storms-the USGS Response to the Hurricanes of 2005. 1306. U.S. Geological Survey Circular, pp. 49–52.
Schneider, A., Friedl, M.A., Potere, D., 2009. A new map of global urban extent from MODIS satellite data. Environ. Res. Lett. 4 (4), 044003.
Schneider, A., Friedl, M.A., Potere, D., 2010. Mapping global urban areas using MODIS 500-m data: new methods and datasets based on 'urban ecoregions. Remote Sens. Environ. 114 (8), 1733–1746.
Sertel, E., Akay, S.S., 2015. High resolution mapping of urban areas using SPOT-5 images and ancillary data. Int. J. Environ. Geol. 2 (2), 63–76.
Seto, S., Iguchi, T., 2007. Rainfall-induced changes in actual surface backscattering cross sections and effects on rain-rate estimates by spaceborne precipitation radar. J. Atmos. Ocean. Technol. 24 (10), 1693–1709.
Seto, K.C., Guneralp, B., Hutyra, L.R., 2012. Global forecasts of urban expansion to 2030 and direct impacts on biodiversity and carbon pools. Proc. Natl. Acad. Sci. 109 (40), 16083–16088.
Seto, K.C., Dhakal, S., Bigio, A., Blanco, H., Delgado, G.C., Dewar, D., Huang, L., Inaba, A., Kansal, A., Lwasa, S., McMahon, J.E., Müller, D.B., Murakami, J., Nagendra, H., Ramaswami, A., 2014. Human settlements, infrastructure and spatial planning. In: Edenhofer, O., Pichs-Madruga, R., Sokona, Y., Farahani, E., Kadner, S., Seyboth, K., Adler, A., Baum, I., Brunner, S., Eickemeier, P., Kriemann, B., Savolainen, J., Schlömer, S., von Stechow, C., Zwickel, T., Minx, J.C. (Eds.), Climate Change 2014: Mitigation of Climate Change. Contribution of Working Group III to the Fifth Assessment Report of the Intergovernmental Panel on Climate Change. Cambridge University Press, Cambridge, United Kingdom and New York, NY, USA.
Shi, K., Huang, C., Yu, B., Yin, B., Huang, Y., Wu, J., 2014. Evaluation of NPP-VIIRS nighttime light composite data for extracting built-up urban areas. Remote Sens. Lett. 5 (4), 358–366.
Small, C., 2001. Estimation of urban vegetation abundance by spectral mixture analysis. Int. J. Remote Sens. 22 (7), 1305–1334.
Small, C., 2005. A global analysis of urban reflectance. Int. J. Remote Sens. 26 (4), 661–681.
Small, C., Elvidge, C.D., 2013. Night on earth: mapping decadal changes of anthropogenic night light in Asia. Int. J. Appl. Earth Obs. Geoinf. 22, 40–52.
Small, C., Nghiem, S.V., 2016. A continuous infrastructure index for mapping human settlements. In: Paper Presented at the 2nd European Association of Remote Sensing Laboratories (EARSeL) Special Interest Group on Land Use and Land Cover (SIG LU/LC) and NASA Land-Cover/Land-Use Change (LCLUC) Joint Workshop, Prague, Czech Republic.
Small, C., Pozzi, F., Elvidge, C.D., 2005. Spatial analysis of global urban extent from DMSP-OLS night lights. Remote Sens. Environ. 96 (3), 277–291.
Small, C., Elvidge, C.D., Balk, D., Montgomery, M., 2011. Spatial scaling of stable night lights. Remote Sens. Environ. 115 (2), 269–280.
Smith, M.O., Ustin, S.L., Adams, J.B., Gillespie, A.R., 1990. Vegetation in deserts: I. A regional measure of abundance from multispectral images. Remote Sens. Environ. 31 (1), 1–26.
Soergel, U., Thoennessen, U., Stilla, U., 2003. Reconstruction of buildings from interferometric SAR data of built-up areas. In: International Archives of Photogrammetry Remote Sensing and Spatial Information Sciences, 34(3/W8), pp. 59–64.
Soh, M.B., 2012. Crime and urbanization: revisited Malaysian case. Procedia. Soc. Behav. Sci. 42, 291–299.
Stevenazzi, S., Masetti, M., Nghiem, S.V., Sorichetta, A., 2015. Groundwater vulnerability maps derived from time dependent method using satellite scatterometer data. Hydrogeol. J. 23 (4), 631–647.
Stevenazzi, S., Bonfanti, M., Masetti, M., Nghiem, S.V., Sorichetta, A., 2017. A versatile method for groundwater vulnerability projections in future scenarios. J. Environ. Manag. 187, 365–374.
Takaku, J., Tadono, T., Tsutsui, K., 2014. Algorithm development of high resolution global DSM generation by ALOS prism. IEEE Geosci. Remote Sens. Symp. 4784–4787.
Taubenbock, H., Felbier, A., Esch, T., Roth, A., Dech, S., 2012. Pixel-based classification algorithm for mapping urban footprints from radar data: a case study for RADARSAT-2. Can. J. Remote. Sens. 38 (3), 211–222.
Tournadre, J., Quilfen, Y., 2003. Impact of rain cell on scatterometer data: 1. Theory and modeling. J. Geophys. Res. 108 (C7), 18.
United Nations, Department of Economic and Social Affairs, Population Division, 2014. World Urbanization Prospects: The 2014 Revision, Highlights (ST/ESA/SER.A/352).
Wu, C., Murray, A.T., 2003. Estimating impervious surface distribution by spectral mixture analysis. Remote Sens. Environ. 84 (4), 493–505.
Xian, G., Homer, C., Dewitz, J., Fry, J., Hossain, N., Wickham, J., 2011. Change of impervious surface area between 2001 and 2006 in the conterminous United States. Photogramm. Eng. Remote. Sens. 77 (8), 758–762.
Yan, W.Y., Shaker, A., El-Ashmawy, N., 2015. Urban land cover classification using airborne LiDAR data: a review. Remote Sens. Environ. 158, 295–310.
Yuan, F., Sawaya, K.E., Loeffelholz, B.C., Bauer, M.E., 2005. Land cover classification and change analysis of the twin cities (Minnesota) metropolitan area by multitemporal

Landsat remote sensing. Remote Sens. Environ. 98, 317–328.
Yusuf, S., Reddy, S., Ounpuu, S., Anand, S., 2001. Global burden of cardiovascular diseases: part I: general considerations, the epidemiologic transition, risk factors, and impact of urbanization. Circulation 104 (22), 2746–2753.
Zha, Y., Gao, J., Ni, S., 2003. Use of normalized difference built-up index in automatically mapping urban areas from TM imagery. Int. J. Remote Sens. 24 (3), 583–594.
Zhang, Q., Seto, K.C., 2013. Can night-time light data identify typologies of urbanization? A global assessment of successes and failures. Remote Sens. 5 (7), 3476–3494.
Zhang, Q., Wang, J., Gong, P., Shi, P., 2003. Study of urban spatial patterns from SPOT panchromatic imagery using textural analysis. Int. J. Remote Sens. 24 (21), 4137–4160.
Zhou, L., Dickinson, R.E., Tian, Y., Fang, J., Li, Q., Kaufmann, R.K., Tucker, C.J., Myneni, R.B., 2004. Evidence for a significant urbanization effect on climate in China. Proc. Natl. Acad. Sci. 101 (26), 9540–9544.
Zhou, Y., Smith, S.J., Zhao, K., Imhoff, M., Thomson, A., Bond-Lamberty, Asrar, G.R., Zhang, X., He, C., Elvidge, C.D., 2015. A global map of urban extent from nightlights. Environ. Res. Lett. 10 (5), 054011.
Zhou, S., Deng, Y.K., Wang, R., Li, N., Si, Q., 2017. Effective mapping of urban areas using ENVISAT ASAR, sentinel-1A, and HJ-1-C data. IEEE Geosci. Remote Sens. Lett. 14 (6), 891–895.